IJMMM
International Journal of
Minerals, Metallurgy and Materials
矿物冶金与材料学报（英文版）

Mineralogical characteristics, metallurgical properties and phase structure evolution of Ca-rich hematite sintering

Lele Niu, Zhengjian Liu, Jianliang Zhang, Dawei Lan, Sida Li, Zhen Li, and Yaozu Wang

Cite this article as:
Lele Niu, Zhengjian Liu, Jianliang Zhang, Dawei Lan, Sida Li, Zhen Li, and Yaozu Wang, Mineralogical characteristics, metallurgical properties and phase structure evolution of Ca-rich hematite sintering, *Int. J. Miner. Metall. Mater.*, 30(2023), No. 2, pp. 303-313. https://doi.org/10.1007/s12613-022-2484-6

View the article online at SpringerLink or IJMMM Webpage.

Articles you may be interested in

Subhnit K. Roy, Deepak Nayak, Nilima Dash, Nikhil Dhawan, and Swagat S. Rath, Microwave-assisted reduction roasting–magnetic separation studies of two mineralogically different low-grade iron ores, *Int. J. Miner. Metall. Mater.*, 27(2020), No. 11, pp. 1449-1461. https://doi.org/10.1007/s12613-020-1992-5

Emile Mukiza, Ling-ling Zhang, and Xiao-ming Liu, Durability and microstructure analysis of the road base material prepared from red mud and flue gas desulfurization fly ash, *Int. J. Miner. Metall. Mater.*, 27(2020), No. 4, pp. 555-568. https://doi.org/10.1007/s12613-019-1915-5

Xiao-liang Zhang, Jue Kou, Chun-bao Sun, Rui-yang Zhang, Min Su, and Shuo-fu Li, Mineralogical characterization of copper sulfide tailings using automated mineral liberation analysis: A case study of the Chambishi Copper Mine tailings, *Int. J. Miner. Metall. Mater.*, 28(2021), No. 6, pp. 944-955. https://doi.org/10.1007/s12613-020-2093-1

Li-xin Qian, Tie-jun Chun, Hong-ming Long, and Qing-min Meng, Detection of the assimilation characteristics of iron ores: Dynamic resistance measurements, *Int. J. Miner. Metall. Mater.*, 27(2020), No. 1, pp. 18-25. https://doi.org/10.1007/s12613-019-1869-7

Hong-fei Wu, Jun-qi Li, Chao-yi Chen, Fei-long Xia, and Zhen-shan Xie, Suspension calcination and alkali leaching of low-grade high-sulfur bauxite: Desulfurization, mineralogical evolution and desilication, *Int. J. Miner. Metall. Mater.*, 27(2020), No. 5, pp. 602-610. https://doi.org/10.1007/s12613-019-1941-3

Xiao-hui Li, Jue Kou, Ti-chang Sun, Shi-chao Wu, and Yong-qiang Zhao, Effects of calcium compounds on the carbothermic reduction of vanadium titanomagnetite concentrate, *Int. J. Miner. Metall. Mater.*, 27(2020), No. 3, pp. 301-309. https://doi.org/10.1007/s12613-019-1864-z

IJMMM WeChat

QQ author group

International Journal of Minerals, Metallurgy and Materials
Volume 30, Number 2, February 2023, Page 303
https://doi.org/10.1007/s12613-022-2484-6

Mineralogical characteristics, metallurgical properties and phase structure evolution of Ca-rich hematite sintering

*Lele Niu*1), *Zhengjian Liu*1), *Jianliang Zhang*1,2), *Dawei Lan*1,4), *Sida Li*1), *Zhen Li*1), *and Yaozu Wang*3),✉

1) School of Metallurgical and Ecological Engineering, University of Science and Technology Beijing, Beijing 100083, China
2) School of Chemical Engineering, The University of Queensland, St Lucia, QLD 4072, Australia
3) Artificial Intelligence Research Institute, University of Science and Technology Beijing, Beijing 100083, China
4) Qinhuangdao Qinye Heavy Industry Group Co., Ltd., Qinhuangdao 066000, China

(Received: 1 January 2022; revised: 20 March 2022; accepted: 28 March 2022)

Abstract: In order to study the sintering characteristics of Ca-rich iron ore, chemical analysis, laser diffraction, scanning electron microscopy, XRD-Rietveld method, and micro-sintering were used to analyze the mineralogical properties and sintering pot tests were used to study the sintering behavior. In addition, a grey correlation mathematical model was used to calculate and compare the comprehensive sintering performance under different calcium-rich iron ore contents. The results demonstrate that the Ca-rich iron ore has coarse grain size and strong self-fusing characteristics with Ca element in the form of calcite ($CaCO_3$) and the liquid phase produced by the self-fusing of the calcium-rich iron ore is well crystallized. Its application with a 20wt% content in sintering improves sinter productivity, reduces fuel consumption, enhances reduction index, and improves gas permeability in blast furnace by 0.45 t/(m^2·h), 6.11 kg/t, 6.17%, and 65.39 kPa·°C, respectively. The Ca-rich iron ore sintering can improve the calorific value of sintering flue gas compared with magnetite sintering, which is conducive to recovering heat for secondary use. As the content of the Ca-rich iron ore increases, sinter agglomeration shifts from localized liquid-phase bonding to a combination of localized liquid-phase bonding and iron oxide crystal connection. Based on an examination of the greater weight value of productivity with grey correlation analysis, the Ca-rich iron ore is beneficial for the comprehensive index of sintering in the range of 0–20wt% content. Therefore, it may be used in sintering with magnetite concentrates as the major ore species.

Keywords: calcium-rich iron ore; mineralogical properties; phase structure evolution; flue gas heat; grey relation analysis

1. Introduction

China has been importing enormous amounts of iron ore to fulfill its local demand of more than one billion tons of steel manufacture every year. According to data from the World Steel Association [1], iron ore imports have surpassed one billion tons since 2016, with the majority coming from Oceania (Australia) and Latin America (Brazil, Peru). Another key reason for iron ore's external dependency is that sinter accounts for more than 70wt% of China's blast furnace charge, and imported hematite and limonite are better suited for sintering production than local iron ore, which typically has low iron grade and high impurity content [2–4].

Although imported iron ore can help achieve better economic and technical indicators for sintering production, the high transportation costs limit the use of imported iron ore, particularly for steel companies in central and western China. A large number of local magnetite concentrates are used, which has adverse effects on the air permeability of the materials layer and the ability to generate liquid phase [5–6]. Many scholars have done plenty of related research in response to these two points [7]. Jiang *et al.* [8–10] proposed composite agglomeration, and Higuchi *et al.* [11–13] developed stand-support sintering, which helped improve the air permeability issue to a certain extent. Many scholars have also studied the fluxing agent optimization and optimized ore blending to improve mixed iron ore's liquid phase generating capacity [14–16]. However, these studies either rely on additional processes and equipment, or the improvement is almost ineffectual.

Recently, the calcium-rich iron ore has been mined in western China. Ca is a very trace element in mainstream iron ores, accounting for less than 0.1wt%, but it has a significant impact on the sintering process, as the mineralization mechanism of sinter is to bond various materials into agglomerates primarily with the Ca-based liquid phase, which is also why different types of fluxes must be added in sintering production [17–18]. Furthermore, the newly discovered Ca-rich iron ore has a coarser particle size after mining that is equal to imported iron ore and hence has the potential to improve air permeability and sintering properties. The impact of Al, Mg, and some other trace elements on the sintering process has been widely researched [19–21]; however, Ca is an element directly connected to the basicity of sinter, resulting in a more

---

✉ Corresponding author: Yaozu Wang E-mail: wgyozu@163.com

complicated influence on the sintering process. Whether the Ca-rich iron ore can improve the negative effects of magnetite concentrates sintering by replacing part of them is a current concern for this Ca-rich iron ore.

The mineralogical characteristics of this Ca-rich iron ore code-named DHS (as an abbreviation of Dahongshan) produced in Xinjiang Uygur Autonomous Region, China were comprehensively analyzed in this study. Then, sintering pot experiments for DHS ore and various other domestic magnetite concentrates were devised. The effects of DHS ore percentage on the sintering process and sinter metallurgical performance were then investigated and compared. Finally, the effects of the Ca-rich iron ore on the mineralization mechanism of the sintered ore were elucidated. This study aims to give a theoretical reference for the practical use of the Ca-rich iron ore.

2. Experimental

2.1. Raw materials

The Ca-rich iron ore and other raw materials, including magnetite concentrates of Yakuang (YK), Rushao (RS), Jinbao (JB), and Dunde (DD), quicklime, and coke breeze, were provided by Xinjiang Bayi Iron and Steel Co., Ltd., China. Table 1 shows their chemical compositions.

2.2. Methods

2.2.1. Sintering pot tests

The sintering pot tests are the fundamental experiment for investigating the sintering performance of iron ores. In this investigation, six sintering pot test schemes were developed (as indicated in Table 2). The Ca-rich iron ore replaces some of the RS and JB magnetite concentrates in varying proportions. Fig. 1 depicts the sintering pot equipment and related experimental parameters of the testing. The raw materials were dispersed into the sintering pot after 6 min of mixing and granulation, and the moisture content was kept at 8.0wt% ± 0.5wt%. The materials layer's thickness was set to 700 mm. The ignition temperature was (1050 ± 50)°C, and the ignition duration was 2 min. During ignition and sintering, the negative pressure regulated by the suction fan were 8 kPa and 10 kPa, respectively. Sinter's binary basicity was set at 1.80. Scheme 0 was introduced to generate return penalties for scheme 1, and all future tests used return fines from the prior test set.

Vertical sintering speed (VSP), yield, sinter productivity (SP), solid fuel consumption (SFC), tumbler index (TI) and flue gas temperature were the significant indicators monitored during the experiment. The flame front velocity as it flows from top to bottom in the materials layer is denoted by *VSP*. The mass ratio of the portion with a particle size higher than 5 mm to the entire sinter output is referred to as yield. SP is used to measure the sinter productivity of sintering machine. The quantity of solid fuel (coke breeze or anthracite) burned per ton of certified sinter is SFC. TI, which represents the cold strength of sinter, is the mass ratio of the sinter greater than 6.3 mm to the total tested sinter after being spun in a drum for 8 min.

2.2.2. Sinter metallurgical performance

Reduction index (RI), low-temperature reduction degradation index (RDI), and softening–melting property (S–M) are metallurgical parameters of sinter that indicate smelting characteristics of successive phases in the ironmaking blast furnace. Their respective test standards are GB/T 13241—2017,

Table 1. Chemical compositions of experimental materials wt%

Material	TFe	FeO	CaO	SiO_2	MgO	Al_2O_3	TiO_2	MnO	S	LOI
DHS	55.91	0.95	10.19	0.33	0.36	0.44	0.02	0.14	0.04	8.24
YK	59.92	28.60	3.09	9.15	1.26	2.05	0.37	0.18	0.23	−2.68
RS	54.74	23.91	0.86	8.69	8.86	1.56	0.12	0.20	0.05	0.74
JB	66.69	28.48	1.07	4.32	0.63	0.55	0.06	0.16	0.10	−2.65
DD	65.51	28.50	2.06	2.07	1.01	1.52	0.15	1.31	0.21	−2.46
Quicklime	0.22	0.05	90.72	4.78	1.25	0.62	0.02	<0.01	0.11	1.68
Coke breeze	0.84	0.95	1.13	6.64	0.33	2.95	0.14	0.02	0.25	86.45

Note: LOI—Loss of ignition.

Table 2. Schemes of sintering pot tests

Scheme	Content / wt%								Basicity
	DHS	YK	RS	JB	DD	Return fines	Quicklime	Coke breeze	
0	5.00	6.90	10.04	52.66	13.84	—	7.16	4.40	1.80
1	5.00	5.50	7.50	42.00	11.00	20.00	5.50	3.50	1.80
2	7.50	5.50	5.63	42.00	11.00	20.00	4.87	3.50	1.80
3	10.00	5.50	3.75	42.00	11.00	20.00	4.25	3.50	1.80
4	12.50	5.50	1.88	42.00	11.00	20.00	3.62	3.50	1.80
5	15.00	5.50	1.88	39.95	11.00	20.00	3.17	3.50	1.80
6	20.00	5.50	1.88	35.84	11.00	20.00	2.28	3.50	1.80

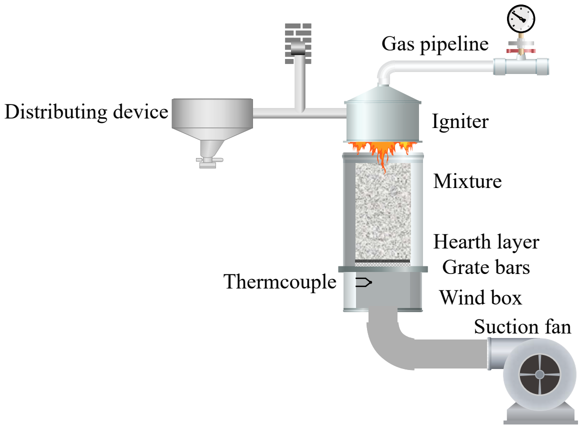

Fig. 1. Sintering pot and the related experimental parameters.

ISO 4696, and GB/T 34211—2017, as shown in Table 3.

The RI expresses reducibility, and the larger the RI, the better the reducibility. The calculation formula is as follows:

$$\mathrm{RI}=\left\{\frac{0.111W_1}{0.430W_2}+\frac{m_1-m_t}{m_0\times 0.430W_2}\times 100\right\}\times 100\% \tag{1}$$

where m_0 is the mass of the sample, g; m_1 is the total mass of the sample and the reduction tube, g; m_t is the total mass of the sample and the reduction tube after reduction t min, g; W_1 and W_2 are the FeO content and the total Fe content of the sample, respectively.

The low-temperature reduction degradation index (RDI) has $\mathrm{RDI}_{+6.3}$, $\mathrm{RDI}_{+3.15}$, and $\mathrm{RDI}_{-0.5}$, which respectively represent the proportions of the portion greater than 6.3 mm, greater than 3.15 mm, and less than 0.5 mm of the reduced sinter after being rotated in a drum with a diameter of 130 mm and a length of 200 mm for 10 min.

The test of softening-melting performance records the displacement curve of the charge and pressure curve in the furnace under the conditions of simulating the blast furnace's temperature, atmosphere, and pressure [22–23]. In addition to the characteristic parameters shown in Table 4, the air permeability index S is also used to characterize the gas permeability of the blast furnace cohesive zone [24–25]:

$$S=\int_{T_\mathrm{s}}^{T_\mathrm{d}} P\,\mathrm{d}T \tag{2}$$

where T_d and T_s represent the melting strat temperature and drip temperature of the iron-bearing charge, P represents the real-time pressure difference inside the furnace, and T represents the real-time temperature of charge.

2.2.3. Mineralogical analysis

Scanning electron microscope with energy dispersive spectroscopy (SEM–EDS, FEI Quanta 250, America) and X-ray diffraction (XRD, Ultima IV, Japan) are also employed to examine the mineral phase structure and mineral composition of the calcium-rich iron ore and produced sinter. In addition, specific auxiliary analytic approaches with full explanations will be employed in the findings and discussions.

Table 3. Testing parameters of metallurgical properties

Property	Sample particle size / mm	Sample weight / g	CO / vol%	CO_2 / vol%	N_2 / vol%	Gas flow / $(\mathrm{L\cdot min^{-1}})$	Reduction temperature / °C	Reduction time / min
RI	10–12.5	500 ± 0.5	30	—	70	15 ± 0.5	900	180
RDI			20	20	60	15 ± 0.5	500	60
S–M			30	—	70	10 ± 0.5	500–1600	190

Table 4. Standard parameters of the softening–melting test under load

Parameter	Meaning
T_{10} / °C	Softening start temperature, the temperature at which the sample shrinks by 10%
T_{40} / °C	Softening end temperature, the temperature at which the sample shrinks by 40%
ΔT_A / °C	Softening temperature range ($T_{40}-T_{10}$)
T_s / °C	Melting start temperature, the temperature when the differential pressure rises sharply
T_d / °C	Drip temperature
ΔT_d / °C	Melting temperature range ($T_\mathrm{d}-T_\mathrm{s}$)

3. Results and discussion

3.1. Mineral properties of calcium-rich iron ore

The magnetite concentrates used for iron ore sintering are usually fine particles with a particle size between -0.074 and 1 mm. The uniform sampling of the DHS ore is carried out for particle size analysis. The cylindrical screen is used for sieving, and then the part of size less than 1 mm is analyzed by a laser analyzer. The result shown in Fig. 2 shows that the particle size of the Ca-rich ore is relatively coarse on the whole, and the part of larger than 1 mm accounts for 69.7wt%. From this perspective, DHS can fully act as the nuclear particle in the mixed magnetite concentrates on helping improve the granulation performance. In the part of less than 1 mm, the part less than 74 μm also occupies a relatively large amount, which may be beneficial to the formation of the bonding phase.

The XRD pattern is shown in Fig. 3. In the analysis process of XRD, trace elements with a content of less than 1wt% are ignored, so the contained minerals of the Ca-rich iron ore DHS can be considered as hematite (Fe_2O_3) and calcite ($CaCO_3$). Ca element is almost all present in DHS in the form of calcite minerals. The results of the quantitative analysis based on the Rietveld method showed that the mass shares of

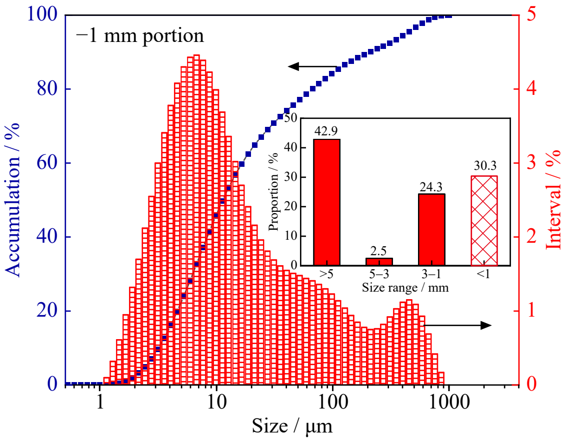

Fig. 2. Particle size distribution of the calcium-rich iron ore DHS: (main image) laser scanning; (inset) sieving.

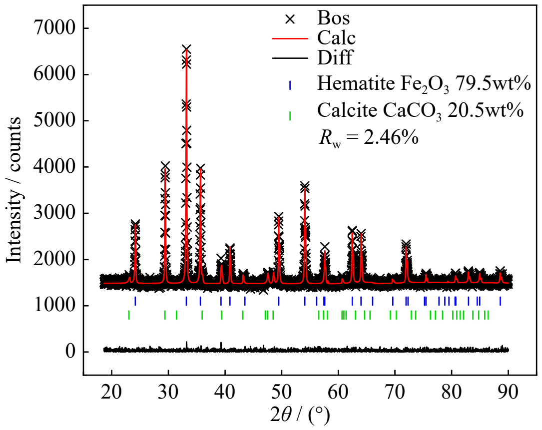

Fig. 3. Rietveld refinement results of DHS.

the two minerals were about 79.5wt% and 20.5wt%, respectively, and the fitting error factor R_w was just 2.46%, which was much less than 10% with high reliability. Similarly, the SEM–EDS images of DHS iron ore also show the same result, as shown in Fig. 4, in which the calcite phase is interspersed with the hematite phase in irregular size and shape, and the two are closely connected. It can be inferred that after ignition, the calcite in DHS will decompose into CaO and CO_2, and react with other oxides in the raw materials to form a liquid phase or a slag phase or something, which correspondingly affect the sintering process and sinter quality. The SEM image also gives the particle morphology of the Ca-rich iron ore, from which it can be seen that the particles have an irregular shape with a small amount of fine particles adhering to the surface. Magnetite typically has smooth flakes that act as adherent powders, whereas limonite has rough spherical shapes of predominantly nuclear particles. Furthermore, magnetite typically has a major mineral composition of Fe_3O_4 and impurity phases containing Si and Mg, resulting in poor assimilation performance. In contrast, limonite frequently contains goethite FeO(OH), which promotes the reaction of iron ore to produce a liquid phase. As a result, the limonite–magnetite mixture is the most popular choice for current sintering production. At this level, the Ca-rich iron ore's granulation and sintering performance are between limonite and magnetite.

Subsequently, the DHS Ca-rich iron ore was ground into

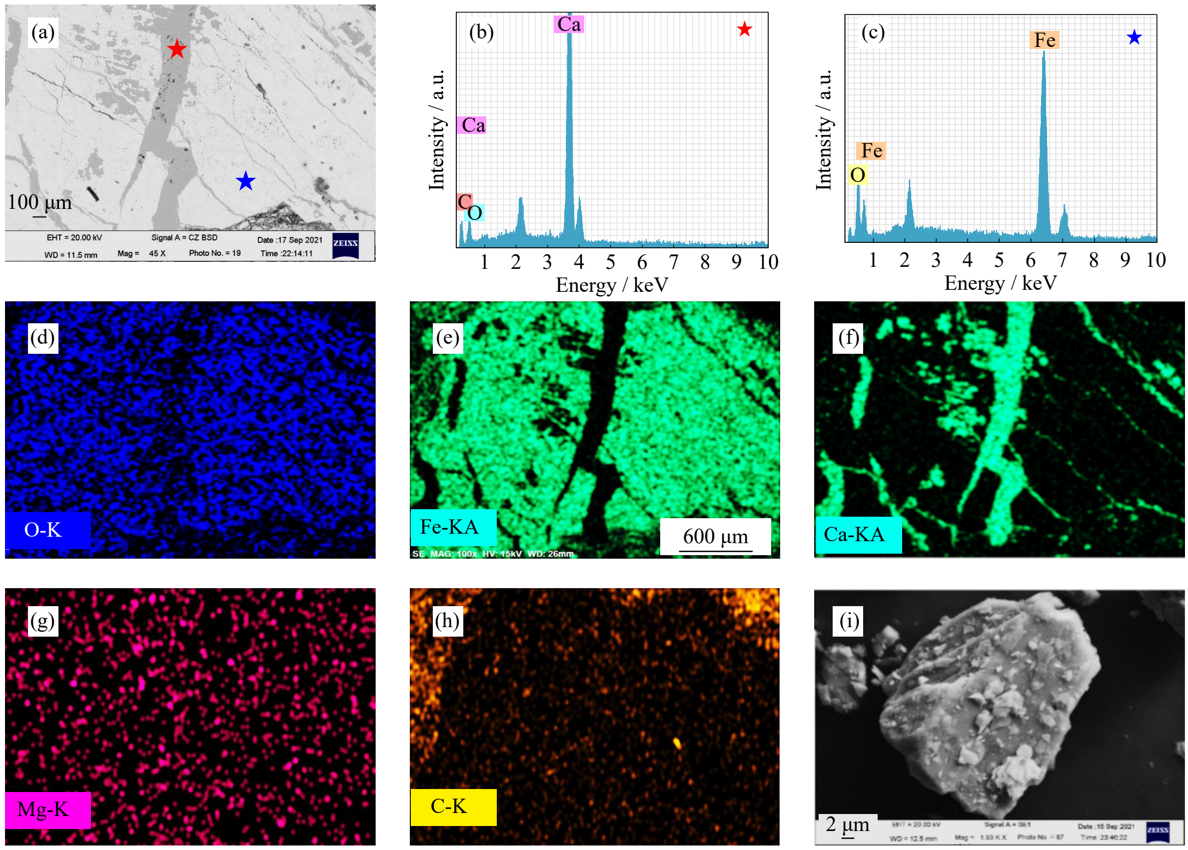

Fig. 4. Mineral phase structure and particle morphology images of DHS: (a) mineral phase image of DHS; (b) EDS analysis of $CaCO_3$; (c) EDS analysis of Fe_2O_3; (d–h) EDS map scanning of O, Fe, Ca, Mg, and C elements; (i) morphology of DHS.

powder with a particle size of 0.074 mm or less, and was then pressed into a cylinder with a diameter of 8 mm using a hydraulic machine at a pressure of 15 MPa for 2 min. Then in an air atmosphere, the cylinder sample was placed in micro sintering equipment and roasted at 1280°C for 5 min. The schematic diagram of the DHS cylinder sample change and the SEM image of the sample after firing is shown in Fig. 5. It can be seen from the mineral phase photos that there are many strips of slag phase. The EDS results show that the light-colored areas are aluminum-containing calcium ferrite (CFA), and the dark areas are monocalcium aluminate (CA). In addition, after the DHS ore is roasted at 1280°C, a large number of cracks appear inside, and many monocalcium aluminate (CA) stripes appear on the surface of the original mineral, which indicates that the DHS calcium-rich iron ore has strong self-reactivity. After the calcite is decomposed, it will form a calcium ferrite liquid phase with the surrounding iron oxides, and the Al element will also be solid-dissolved to participate in the formation of the slag phase [26]. The effects of this phenomenon on the property of the bonding phase in the sintering process are worthy of attention.

3.2. Sintering process, sinter metallurgical properties and phase structure

This chapter will discuss the effects of the DHS calcium-rich iron ore content on the economic and technical indicators of the sintering process, sinter metallurgical properties, and mineralogy. Table 5 shows the chemical composition of sinters with different DHS Ca-rich iron ore contents. The MgO and Al_2O_3 contents of sinter are reduced after the replacement of RS and JB by the Ca-rich hematite due to the low gangue element content.

3.2.1. Sintering process

Fig. 6 shows the economic and technical indicators of the sintering process under different DHS contents, including vertical sintering speed (VSP), yield, sinter productivity (SP), solid fuel consumption (SFC) and tumbler index (TI). Due to the better granulation performance of DHS brought by the

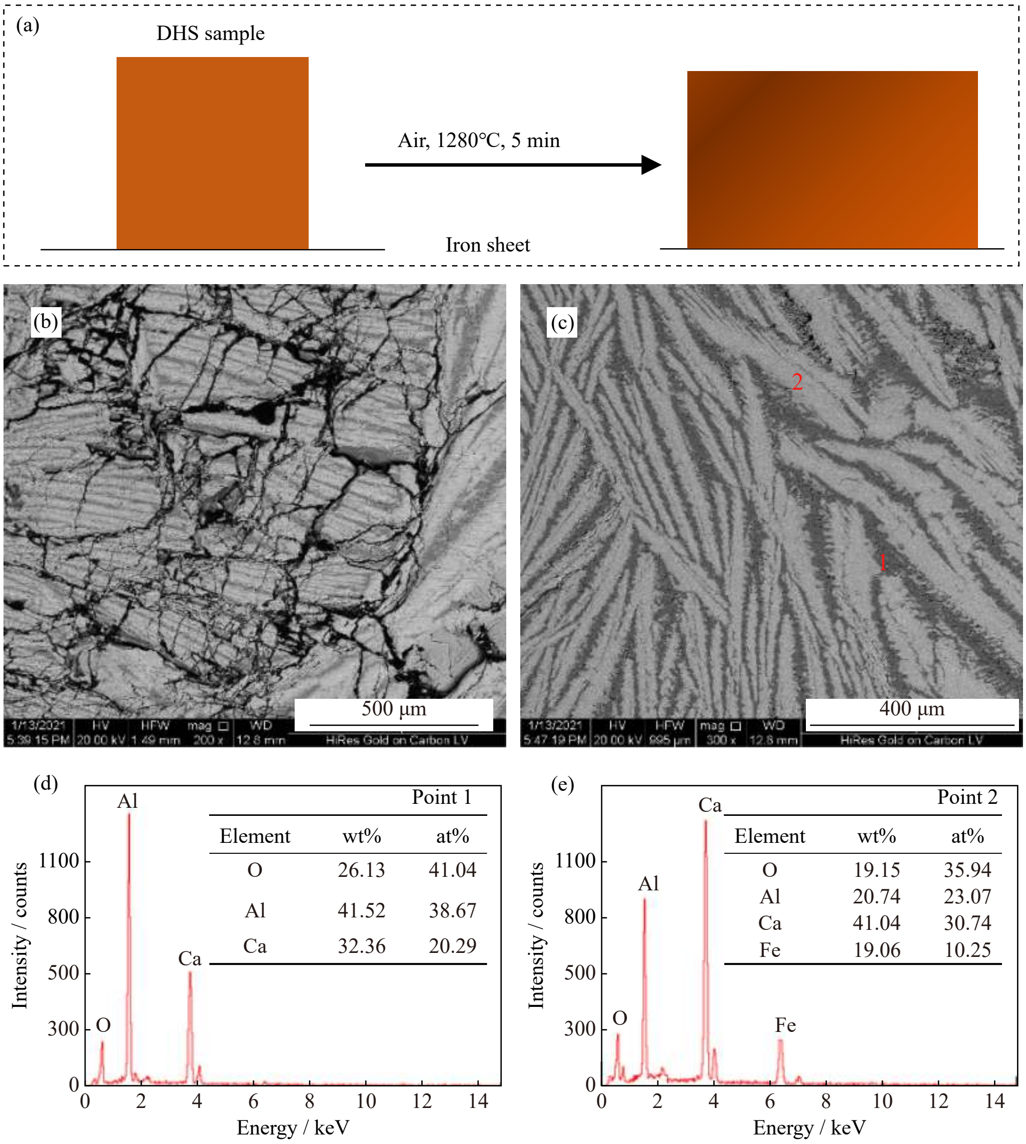

Point 1

Element	wt%	at%
O	26.13	41.04
Al	41.52	38.67
Ca	32.36	20.29

Point 2

Element	wt%	at%
O	19.15	35.94
Al	20.74	23.07
Ca	41.04	30.74
Fe	19.06	10.25

Fig. 5. Schematic diagram of DHS roasted at 1280°C and mineral phase transformation: (a) roasting changes of DHS; (b, c) mineral phase image of the roasted sample; (d) EDS analysis of CA; (e) EDS analysis of CFA.

Table 5. Chemical compositions of magnetite sinter with different Ca-rich iron ore contents

Scheme	DHS content / wt%	Chemical composition / wt%								Basicity
		TFe	CaO	SiO_2	MgO	Al_2O_3	TiO_2	MnO	S	
1	5.00	57.93	8.64	4.80	1.60	1.02	0.11	0.27	0.13	1.80
2	7.50	58.48	8.28	4.60	1.42	0.99	0.10	0.27	0.13	1.80
3	10.0	59.10	7.87	4.37	1.21	0.97	0.10	0.27	0.12	1.80
4	12.50	59.74	7.45	4.14	0.99	0.94	0.10	0.27	0.12	1.80
5	15.00	60.08	7.18	3.99	0.94	0.93	0.10	0.27	0.12	1.80
6	20.00	60.55	6.77	3.76	0.91	0.93	0.10	0.27	0.12	1.80

coarser particles than magnetite concentrates, the vertical sintering speed increases significantly (from 17.83 to 21.98 mm/min) with the increase of the DHS content, which means better air permeability in the materials layer. The overall yield also has an upward trend. The combined effect of the improvement of the vertical sintering speed and the yield has promoted a significant increase of 0.45 t/(m^2·h) in the sinter productivity, which is the most concerned index in current sintering production. The solid fuel consumption has also decreased due to the increase in the sinter productivity. When the DHS content increases from 0 to 20wt%, the solid fuel consumption drops by 6.11 kg/t, which would bring substantial economic and environmental benefits to a medium-sized sintering machine with a daily output of about 10000 t. However, the tumbler index of sinter shows a downward trend as the DHS content increases. When the Ca-rich iron ore content increases, the additional CaO content added during the sintering process decreases accordingly, so that most of the calcium ferrite liquid phase appears around the Ca-rich iron ore, and the other regions are mainly hematite grains. Moreover, the strength of hematite (260.70 N/mm^2) is lower than that of calcium ferrite (370.11 N/mm^2), which leads to the reduction of TI.

3.2.2. Flue gas calorific value

The heat resource of sintering flue gas is the critical heat income for modern steel companies to establish an energy cycle system, and changes in the raw materials have a significant impact on the flue heat. The thermocouple inside the wind box of the sintering pot monitors the exhaust gas temperature during the sintering process. To effectively reflect the temperature difference of exhaust gas during the sintering process, the flue gas heat index (Q) is defined as Eq. (3):

$$Q=\int_{t_0}^{t_1} T\,\mathrm{d}t \tag{3}$$

where t_0 refers to the time when the exhaust gas temperature starts to rise rapidly, subject to the time with a temperature higher than 60°C; t_1 is the end time of sintering, subject to the time when exhaust gas temperature starts to drop; T is the exhaust gas temperature during the sintering process. The integration of the temperature in the flue gas over a high-temperature duration can characterize the calorific value contained in the flue gas.

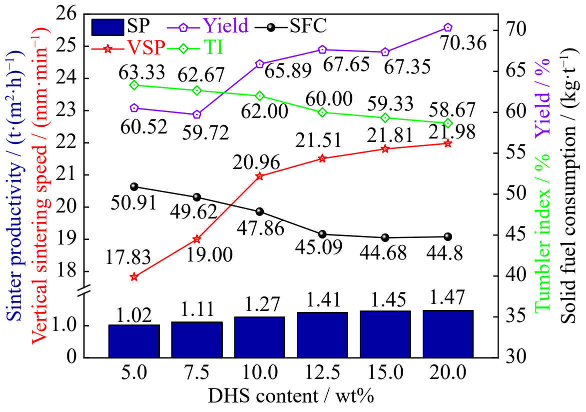

Fig. 6. Economic–technical indicators of sintering process.

Fig. 7 shows the exhaust gas temperature curve of the sintering process and the calculated Q values under different DHS contents. The results show an approximately linear relationship between the Q value and the DHS calcium-rich ore content, indicating a significant influence of the Ca-rich hematite on the exhaust gas temperature during the sintering process. When the DHS content increases from 5wt% to 20wt%, the Q value increases from 652.75 to 2376.24°C·min. It is known that $CaCO_3$ decomposition is endothermic, and magnetite oxidation is exothermic. After the content of the Ca-rich ore increases to replace part of the magnetite, the heat in the exhaust gas is instead elevated, so it is presumed that two factors, fuel combustion efficiency and sintering layer heat transfer efficiency, produce changes. The newborn CaO decomposed by calcite in the calcium-rich iron ore has higher activity, which can promote the improvement of fuel combustion efficiency; on the other hand, as the content of DHS increases, the amount of externally added CaO decreases, and the generated liquid phase is relatively more concentrated, which reduces the resistance to heat transfer. Solid fuel consumption is reduced when the calcium-rich iron ore is used in sintering. Still, the heat in the sintering exhaust gas increases, which has a favorable impact on heat recycling and carbon-emission reduction in steel businesses.

3.2.3. Sinter metallurgical performance

Fig. 8 shows the reduction index (RI) and the sinter's low-temperature reduction degradation index (RDI) under different DHS contents. It can be seen that the reducibility of these groups of sinter has improved with the increase of the DHS content, but there is no longer apparent upward trend after the content reaches 12.5wt% and higher. When the Ca-rich iron ore content is increased from 0% to 20%, the reduction index improves by 6.17%. As for the RDI, it can be seen that the proportions larger than 3.15 and 6.3 mm both decrease, and

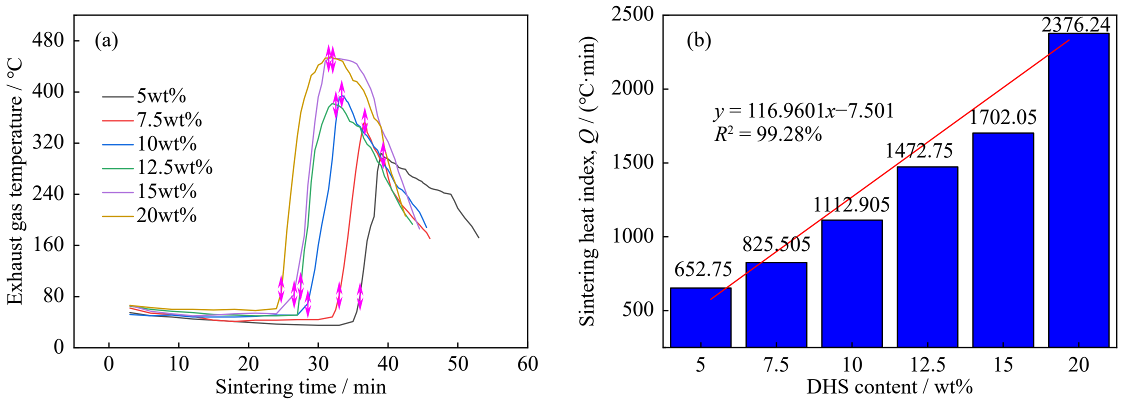

Fig. 7. (a) Exhaust gas temperature curves of the sintering process and (b) the calculated Q values under different DHS contents.

the proportion smaller than 0.5mm rises, which means that as the proportion of DHS increases, more pulverization occurs during the reduction process. The slight increase in reducibility is mainly attributed to the lower Mg content of sinter after DHS replaces high Mg magnetite. The reason for the deterioration of the low-temperature reduction degradation performance is that after the DHS content increases, there are more hematite grains in the sinter, which aggravates the degradation phenomenon occurring in the reduction process of Fe_2O_3 to Fe_3O_4; on the other hand, as the content of the DHS Ca-rich ore increases, the amount of quicklime added in the sintering process decreases due to the fixed basicity of 1.8. Thus the sintering environment of magnetite is low-basicity. The formation conditions of calcium ferrite are poor, and silicates or calcium-iron olivine will be generated more readily than calcium ferrite, which reduces the structural strength of the sinter and deteriorates the ability to withstand the lattice stress during the reduction process.

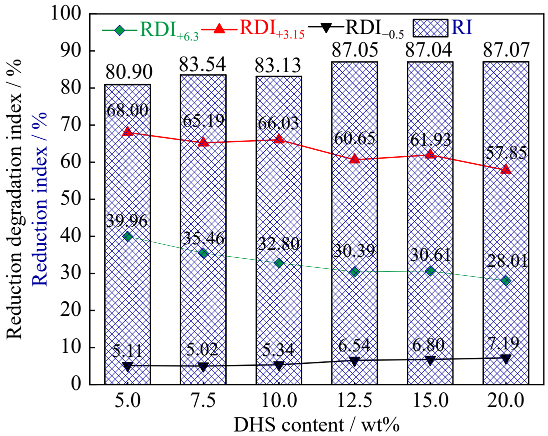

Fig. 8. Reduction degradation index and reduction index under different DHS contents.

Fig. 9 shows the characteristic parameters of softening–melting performance of sinter under different DHS contents. The softening start temperature T_{10} shows a downward trend, from 1233°C at 5wt% DHS to 1169°C at 20wt% DHS. This is because as the proportion of DHS increases, the reducibility improves. Before reaching the cohesive zone, more FeO can be reduced, generating more low-melting-point compounds, and lowering the softening temperature of the sinter, which will delay the entry of the sinter to the indirect reduction stage and is not conducive to reducing the coke ratio to a certain extent. However, the melting temperature range is gradually narrowed; that is, the dripping of slag and iron occurs soon after the pressure in the furnace rises, which means that the gas flow is not subject to long-term or considerable resistance.

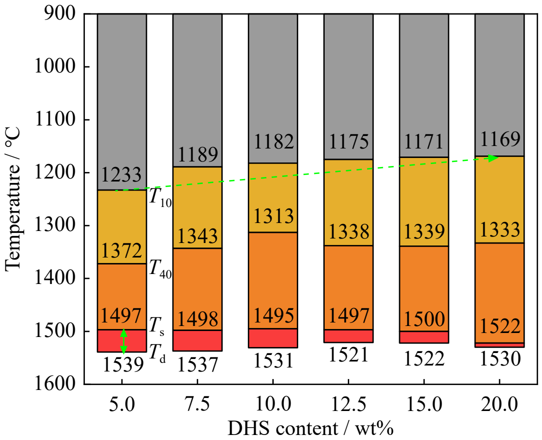

Fig. 9. Characteristic parameters of softening–melting performance under different DHS contents.

Furthermore, according to Eq. (2), the air permeability index of the sinter during the softening–melting process is calculated. It can be seen from Fig. 10 that with the increase in the content of the Ca-rich ore, the S value of the sinter decreases significantly with an amplitude of 65.39 kPa·°C, and the air permeability of the cohesive zone is significantly improved, which is essential for the stability and efficiency of the blast furnace smelting.

3.2.4. Sinter phase structure evolution

Scanning electron microscopy (SEM) was used to examine the microstructure of the sinter with varying DHS contents. When the DHS contents are 5wt% and 7.5wt%, the mineral phase reveals interweaving of acicular calcium ferrite and hematite grains, as seen in Fig. 11. When the DHS content is further increased, the calcium ferrite concentration reduces dramatically over a large region due to a reduction in the applied CaO flux. The needle-like structure changes to strip-like. When the DHS content reaches 20wt%, most hematite grains no longer have a calcium ferrite phase between

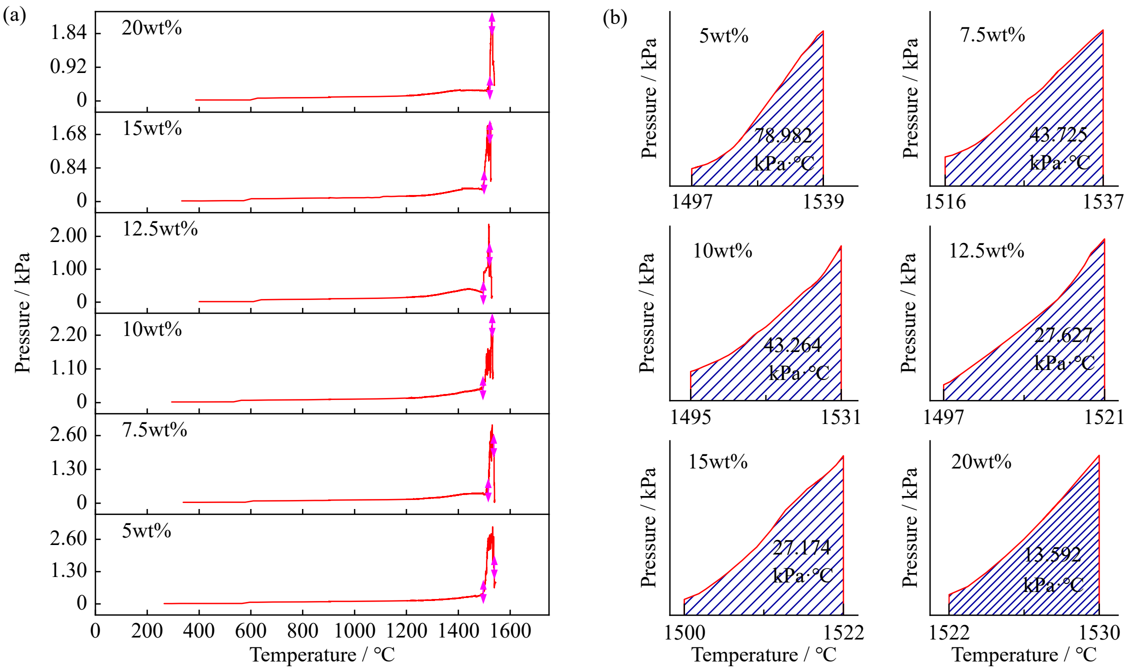

Fig. 10. (a) Pressure difference curves and (b) air permeability indexes under different DHS contents.

them, and these grains are linked by a small amount of calcium-iron olivine (kirschsteinite) or connect with themselves, which is also an important reason for the sinter tumbler index to decrease. Fig. 12 depicts a schematic depiction of the fluctuation of the sinter phase structure with the DHS content. The Calcium-rich iron ore serves as a flux to some extent. When no calcium-rich ore is supplied, the tiny flux particles scatter in the sintering mixture and assimilate with the iron ore to generate a liquid phase. Liquid phase bonding is the most critical approach to aggregate the mixture into agglomerates. When the calcium-rich iron ore is added to the sintering mixture, it is equivalent to a portion of the flux dispersed inside the iron ore. In this case, the Ca-rich iron ore generates more calcium ferrite liquid phase in the region around itself, while CaO brought by the added quicklime disperses in the mixture generates more kirschsteinite, and the phenomenon of Fe_2O_3 crystal connection appears between the iron oxides grains. Thus, after using the calcium-rich iron ore, the sintering mixture is agglomerated into blocks in a manner that includes liquid-phase bonding and iron oxide crystal connection. As a result of the utilization of the calcium-rich iron ore, the sintering mixture is agglomerated into blocks via localized liquid-phase bonding and iron oxide crystal connection.

Apparently, with the increase of the Ca-rich hematite content, the distribution of the calcium ferrite phase in the sinter cake is more uniform. The iron oxide crystal connection and calcium-iron olivine bonding also help to agglomerate. As a result, the yield of the sinter is improved, and accordingly, the sinter productivity is increased, and the solid fuel consumption is reduced. However, at the same time, the insufficient crystal connection and the local decrease in the concentration of calcium ferrite make the sinter slightly less strong when subjected to external forces, which leads to a reduction in the tumbler index.

3.3. Optimization of DHS content during sintering with iron concentrates

Although the emergence of the Ca-rich iron ore DHS is important for sintering production, the experimental test and analysis results show that the increase of DHS content has a possible good or harmful impact on the economic and technical index of sintering and the metallurgical performance of sinter, which also means that a comprehensive ranking of the different DHS contents is needed to guide sintering with iron concentrates. Grey correlation analysis has been widely used in engineering fields and is suitable for comparing the merits of variable values based on the results relied upon [27–28].

In this study, seven evaluation indexes were selected. Each indicator is assigned a weight value [29]: yield (10%), sinter productivity (20%), tumbler index (10%), solid fuel consumption (15%), reduction index (15), reduction degradation index $RDI_{+3.15}$ (15%), and softening–melting permeability index S (15%). The matrix consisting of the optimal values of these seven indicators in the six sets of experiments is [70.36, 1.47, 63.33, 44.68, 80.90, 68.00, 13.592]. Thus, it is necessary to calculate the grey correlation between the matrix consisting of seven indicators for each group of tests and this optimal matrix according to Eq. (4). The higher the correlation, the more optimal the indicators are for that group of tests.

$$r_t = \sum_{k=1}^{m}[\varepsilon_t(k)\,\omega_k] \Big/ \sum_{k=1}^{m}\omega_k \qquad (4)$$

where $\varepsilon_t(k)$ and ω_k represent each index's correlation coefficient and weight value, respectively. k ($k = 1, 2, 3, \ldots, m$) represents each index, and there are 7 indexes in this study. r_t is used to characterize the relation between the reference sequence and the comparison sequence.

After the steps of dimensionless processing and differ-

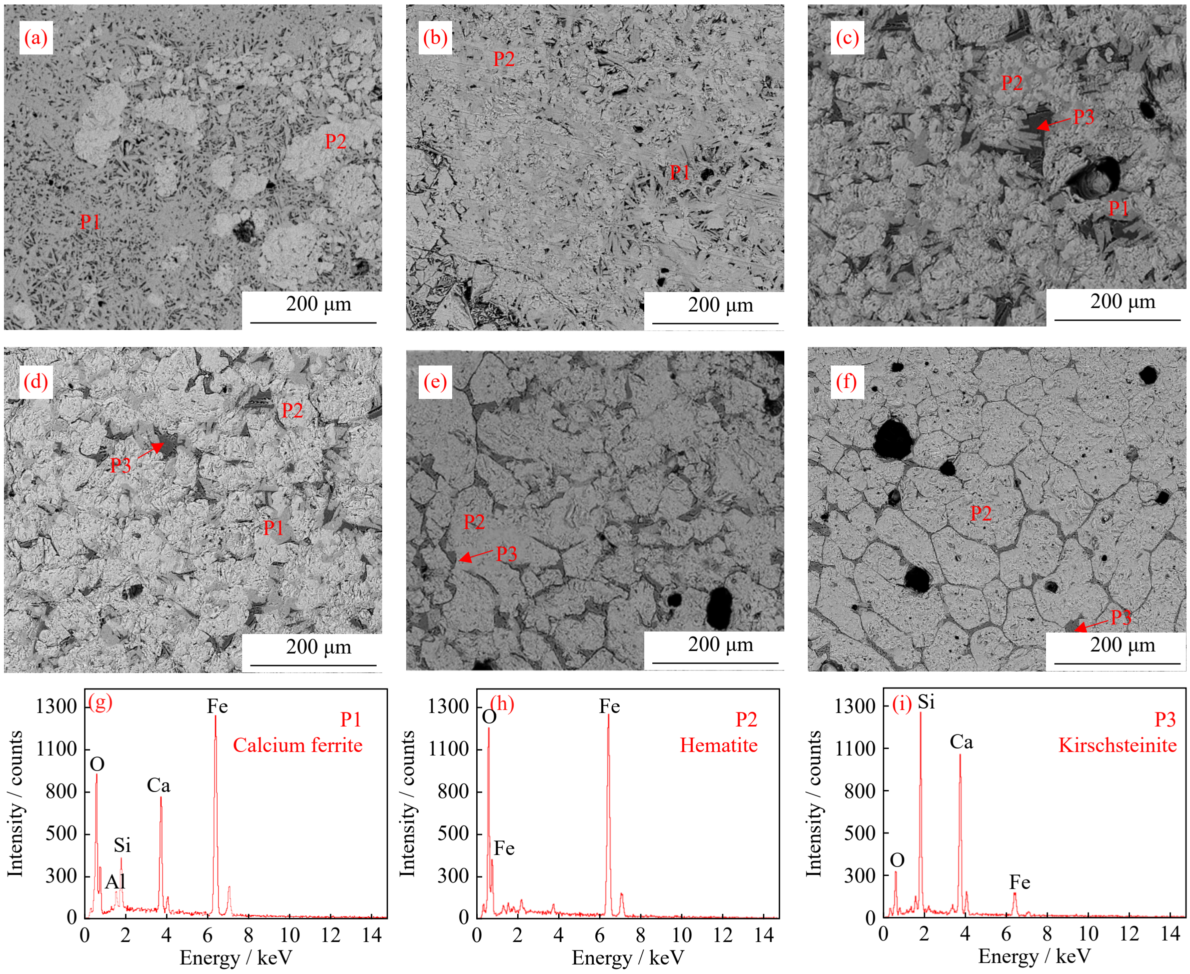

Fig. 11. Microstructures of sinter with different DHS contents: (a) 5wt%; (b) 7.5wt%; (c) 10wt%; (d) 12.5wt%; (e) 15wt%; (f) 20wt%. EDS analysis results of (g) calcium ferrite, (h) hematite, and (i) kirschsteinite.

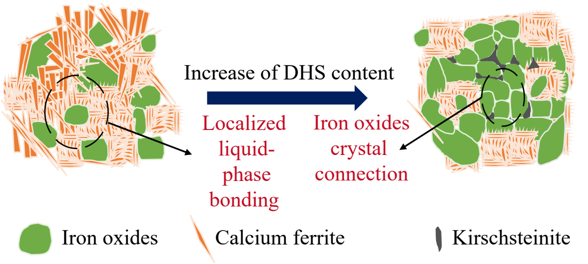

Fig. 12. Schematic diagram of sinter phase structure with an increase in the DHS content.

ence calculation, the calculated grey correlation is shown in Fig. 13. It can be seen that with the set weight values as described above, the correlation between the six groups of experimental indicators and the optimal indicators gradually increases, and the indicators show an overall optimum at 20wt% DHS content. This also means that the calcium-rich DHS ore can be used as the main ore species in sintering with concentrates. It is important to note that the correlation degree calculation is based on the weight value assigned to each indicator. After discussion with the iron and steel companies, we have given higher weight to these indicators as they are now paying more attention to the yield, sinter productivity, and solid fuel consumption indicators due to the environmental restrictions.

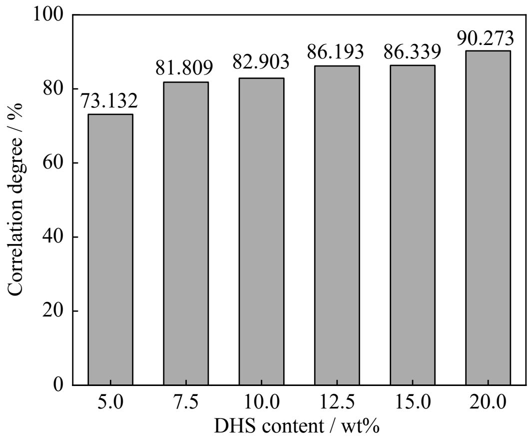

Fig. 13. Grey correlation degree between indicators of each content and the optimal.

4. Conclusions

In this paper, the effects of the Ca-rich type iron ore on the sintering process with magnetite concentrates were carefully studied, and the following conclusions can be obtained.

(1) This Ca-rich iron ore is coarse-grained, with the +5 mm fraction accounting for 42.9wt%, much greater than typical iron concentrates. Ca is contained in this ore in the

form of calcite ($CaCO_3$). This iron ore self-melts at 1280°C and internal assimilation processes yield a substantial amount of streaky aluminum-bearing calcium ferrite.

(2) As the content of the calcium-rich ore grows, the vertical sintering speed increases significantly, the sinter productivity and yield increase, and the solid fuel consumption and tumbler index decrease. Furthermore, the Ca-rich iron ore sintering can improve the calorific value of sintering flue gas compared with magnetite sintering, which is conducive to recovering heat for secondary use. The total heat exhibits an essentially linear connection with the calcium-rich ore content. In terms of metallurgical properties, when the calcium-rich ore content increases, the reducibility is improved and the reduction degradation performance deteriorates. The cohesive zone's air permeability index exhibits a marked decreasing tendency, and the values are all relatively low, which is highly good for blast furnace downstream. Compared with magnetite concentrates sintering, the addition of 20wt% Ca-rich hematite content improves sinter productivity, reduces fuel consumption, enhances reduction index, and improves air permeability in blast furnace by 0.45 $t/(m^2 \cdot h)$, 6.11 kg/t, 6.17%, and 65.39 kPa·°C, respectively.

(3) As the content of the calcium-rich ore increases, the calcium-rich ore is self-melted initially to produce a considerable volume of the liquid phase. At the same time, the flux in the mixture mainly forms calcium-iron olivine. The sinter agglomeration shifts from localized liquid-phase bonding to a mix of localized liquid-phase bonding and iron oxide crystal connection.

(4) The ranking of sintering indices for each calcium-rich ore content was computed using grey correlation analysis with the goal of increasing sinter production in mind. The results demonstrate that when the calcium-rich ore content increases in the range of 5wt%–20wt%, the overall sintering index steadily improves, indicating that the calcium-rich ore is acceptable for use as the major ore species in sintering with iron concentrates.

Acknowledgement

This work was financially supported by the National Natural Science Foundation of China (No. 52174291).

Conflict of Interest

No potential conflict of interest was reported by the authors.

References

[1] World Steel Association, *World Steel in Figures 2017* [2017-05-29]. https://worldsteel.org/zh-hans/steel-topics/statistics/world-steel-in-figures/

[2] X. Bo, Z.L. Li, J.B. Qu, *et al.*, The spatial-temporal pattern of sintered flue gas emissions in iron and steel enterprises of China, *J. Cleaner Prod.*, 266(2020), p. 121667.

[3] L.X. Yang and L. Davis, Assimilation and mineral formation during sintering for blends containing magnetite concentrate and hematite/pisolite sintering fines, *ISIJ Int.*, 39(1999), No. 3, p. 239.

[4] D.H. Liu, H. Liu, J.L. Zhang, *et al.*, Basic characteristics of Australian iron ore concentrate and its effects on sinter properties during the high-limonite sintering process, *Int. J. Miner. Metall. Mater.*, 24(2017), No. 9, p. 991.

[5] H.L. Han and L.M. Lu, Recent advances in sintering with high proportions of magnetite concentrates, *Miner. Process. Extr. Metall. Rev.*, 39(2018), No. 4, p. 217.

[6] J.M.F. Clout and J.R. Manuel, Fundamental investigations of differences in bonding mechanisms in iron ore sinter formed from magnetite concentrates and hematite ores, *Powder Technol.*, 130(2003), No. 1-3, p. 393.

[7] V.D.M. Oliveira, V.G. de Resende, A.L.A. Domingues, M.C. Bagatini, and L.F.A. de Castro, Alternative to deal with high level of fine materials in iron ore sintering process, *J. Mater. Res. Technol.*, 8(2019), No. 5, p. 4985.

[8] T. Jiang, G.H. Li, H.T. Wang, K.C. Zhang, and Y.B. Zhang, Composite agglomeration process (CAP) for preparing blast furnace burden, *Ironmaking Steelmaking*, 37(2010), No. 1, p. 1.

[9] T. Jiang, L.P. Xu, Q. Zhong, *et al.*, Efficient preparation of blast furnace burdens from titanomagnetite concentrate by composite agglomeration process, *JOM*, 73(2021), No. 1, p. 326.

[10] T. Jiang, Z.W. Yu, Z.W. Peng, M.J. Rao, Y.B. Zhang, and G.H. Li, Preparation of BF burden from titanomagnetite concentrate by composite agglomeration process (CAP), *ISIJ Int.*, 55(2015), No. 8, p. 1599.

[11] K.I. Higuchi, T. Kawaguchi, M. Kobayashi, *et al.*, Improvement of productivity by stand-support sintering in commercial sintering machines, *ISIJ Int.*, 40(2000), No. 12, p. 1188.

[12] L. Lu and O. Ishiyama, Recent advances in iron ore sintering, *Miner. Process. Extr. Metall.*, 125(2016), No. 3, p. 132.

[13] Y.Z. Wang, Z.J. Liu, J.L. Zhang, Y.P. Zhang, L.L. Niu, and Q. Cheng, Study of stand-support sintering to achieve high oxygen potential in iron ore sintering to enhance productivity and reduce CO content in exhaust gas, *J. Cleaner Prod.*, 252(2020), art. No. 119855.

[14] D. Fernández-González, I. Ruiz-Bustinza, J. Mochón, C. González-Gasca, and L.F. Verdeja, Iron ore sintering: Environment, automatic, and control techniques, *Miner. Process. Extr. Metall. Rev.*, 38(2017), No. 4, p. 238.

[15] T.C. Ooi, S. Campbell-Hardwick, D.Q. Zhu, and J. Pan, Sintering performance of magnetite-hematite-goethite and hematite-goethite iron ore blends and microstructure of products of sintering, *Miner. Process. Extr. Metall. Rev.*, 35(2014), No. 4, p. 266.

[16] J.L. Zhang, Z.W. Hu, H.B. Zuo, Z.J. Liu, Z.X. Zhao, and T.J. Yang, Ore blending ratio optimisation for sintering based on iron ore properties and cost, *Ironmaking Steelmaking*, 41(2014), No. 4, p. 279.

[17] N.A.S. Webster, M.I. Pownceby, I.C. Madsen, and J.A. Kimpton, Silico-ferrite of calcium and aluminum (SFCA) iron ore sinter bonding phases: New insights into their formation during heating and cooling, *Metall. Mater. Trans. B*, 43(2012), No. 6, p. 1344.

[18] M.I. Pownceby and J.M.F. Clout, Importance of fine ore chemical composition and high temperature phase relations: Applications to iron ore sintering and pelletising, *Miner. Process. Extr. Metall.*, 112(2003), No. 1, p. 44.

[19] S.W. Kim, J.W. Jeon, I.K. Suh, and S.M. Jung, Improvement of sintering characteristics by selective granulation of high Al_2O_3 iron ores and ultrafine iron ores, *Ironmaking Steelmaking*, 43(2016), No. 7, p. 500.

[20] L.S. Li, J.B. Liu, X.R. Wu, X. Ren, W.B. Bing, and L.S. Wu, Influence of Al_2O_3 on equilibrium sinter phase in N_2 atmosphere, *ISIJ Int.*, 50(2010), No. 2, p. 327.

[21] T. Umadevi, P.C. Mahapatra, and M. Prabhu, Influence of MgO addition on microstructure and properties of low and high silica iron ore sinter, *Miner. Process. Extr. Metall.*, 122(2013), No. 4, p. 238.

[22] Y. Hosotani, K. Yamaguchi, T. Orimoto, K.I. Higuchi, T. Kawaguchi, and H. Goto, Development of evaluation method for softening-melting properties of sinter, *Tetsu-to-Hagane*, 83(1997), No. 2, p. 97.

[23] Y.N. Qie, Q. Lyu, X.J. Liu, *et al.*, Effect of hydrogen addition on softening and melting reduction behaviors of ferrous burden in gas-injection blast furnace, *Metall. Mater. Trans. B*, 49(2018), No. 5, p. 2622.

[24] S.L. Wu, Y.N. Lu, Z.B. Hong, and H. Zhou, Improving the softening and melting properties of ferrous burden with high Al_2O_3 content for blast furnace by ore blending, *ISIJ Int.*, 60(2020), No. 7, p. 1504.

[25] S.L. Wu, W. Huang, M.Y. Kou, X.L. Liu, K.P. Du, and K.F. Zhang, Influence of Al_2O_3 content on liquid phase proportion and fluidity of primary slag and final slag in blast furnace, *Steel Res. Int.*, 86(2015), No. 5, p. 550.[LinkOut].

[26] Y.X. Xue, J. Pan, D.Q. Zhu, *et al.*, Effect of alumina occurrence on sintering performance of iron ores and its action mechanism, *J. Mater. Res. Technol.*, 12(2021), p. 1157.[LinkOut].

[27] D.H. Liu, J.L. Zhang, Z.J. Liu, Y.Z. Wang, X. Xue, and J. Yan, Effects of iron sand ratios on the basic characteristics of vanadium titanium mixed ores, *JOM*, 68(2016), No. 9, p. 2418.

[28] J. E, Y. Zeng, Y. Jin, *et al.*, Heat dissipation investigation of the power lithium-ion battery module based on orthogonal experiment design and fuzzy grey relation analysis, *Energy*, 211(2020), art. No. 118596.

[29] Z.J. Liu, L.L. Niu, S.J. Zhang, *et al.*, Comprehensive technologies for iron ore sintering with a bed height of 1000 mm to improve sinter quality, enhance productivity and reduce fuel consumption, *ISIJ Int.*, 60(2020), No. 11, p. 2400.